

## Structural comparisons of the species of recognition of Ni<sup>2+</sup>, Cu<sup>2+</sup>, Zn<sup>2+</sup>, Cd<sup>2+</sup>, Hg<sup>2+</sup> and Ag<sup>+</sup> with 1,3-di-conjugates of calix[4]arene by DFT computations

Balaji Ramanujam, Jugun Prakash Chinta & Chebrolu P Rao\*

Bioinorganic Laboratory, Department of Chemistry, Indian Institute of Technology Bombay, Powai, Mumbai 400 076, India  
Email: cprao@iitb.ac.in

Received 22 August 2011

Calixarenes are versatile macromolecular systems, which would exhibit better host-guest chemistry upon appropriate derivatization. Our group has been involved in the synthesis of a variety of calix[4]arene conjugates, which were found to selectively recognize metal ions. Though such recognitions have been demonstrated, based on different experimental studies, the qualitative and semi-quantitative understanding of the coordination aspects are still lacking owing to the non-availability of the crystal structures of the species of recognition. Hence, in order to understand the coordination chemistry of the interactions between the host calix[4]arene receptor and the guest metal ion species, computational modelling studies have been carried out. In this regard, five conjugates of calix[4]arene, which are 1,3-di-O-derivised at the lower-rim and appended over an amide as well as Schiff base linker have been studied. The computational modelling studies have been carried out at the level of density functional theory to yield coordination geometries, which are intune with the experimental observations and comparable to those reported in the literature in the case of similar receptor systems. The species of recognition obtained with the metal ions are found to have some structural resemblances with the metal sites present in metalloproteins. The modelling studies and the coordination geometries are discussed in this article.

**Keywords:** Density functional calculations, Calix[4]arene conjugates, Macromolecules, Species of recognition, Coordination core, Computational modelling

Calix[n]arenes are macrocyclic molecules made of 'n' number of phenol units connected by *ortho* methylene bridge centers.<sup>1</sup> Calix[4]arenes are the simplest, and most common examples of this family, with four phenolic residues being present in the macrocyclic ring that provides a platform for organic derivatization. Reactions of simple calix[4]arene with transition metal complexes can produce metal phenolates with substitution of one to four hydrogen atoms.<sup>2</sup> Derivatives of calix[4]arenes have been extensively studied in the recent times, for their conformational flexibility, derivatisability and complexing ability. Thus, calix[4]arene conjugates have been exploited in a variety of chemical applications, including catalysis, host-guest chemistry, separation chemistry, selective ion transport, and sensors.<sup>1(d)</sup> Calix[4]arene can exist in four conformations designated as cone, partial cone, 1,2- alternate, and 1,3-alternate. It is well documented that the introduction of bulky substituents at the lower rim will impart conformational immobilization to these derivatives. Any of these conformations represents a special three-dimensional arrangement with different complexation behaviours and hence

with potential applications as a molecular scaffold and advantageously provide useful building blocks in supramolecular chemistry.

It is known in the literature that the calixarene-conjugates are expected to form host-guest complexes by exhibiting a variety of ensembles.<sup>3</sup> Apart from the experimental determination of these conjugates for their applicability, the structural features of the complexes formed are also important for understanding the details of binding. In the absence of crystal structures, there exists a dire need to model the structure of the species of recognition or the complexation with the experimental clues available to improve the understanding. In this regard, computational modelling is one of the useful and affordable means of predicting the structure. In recent years, computational investigations of these compounds have revealed that calix[4]arenes provide a congenial platform for the design of new systems with improved properties, and also to interpret their chemical and physical properties.<sup>4</sup> During the past few years, our group has been actively involved in the design and development of the conjugates of calix[4]arene to sense ions of biological and

environmental importance by selectively bringing about synthetic modifications such that the resultant conjugates possess suitable binding core(s).<sup>5</sup> The focus of the present article is the computational modeling of the species of recognition of these calixarene conjugates towards different metal ions of biological importance to provide structural features for such selective recognition.

## Methodology

### Computation and visualisation tools

All geometry optimization calculations<sup>6</sup> of the complexes of the conjugates of calixarenes (species of recognition) were carried out using Gaussian 98 or 03. The visualization and input preparations were done using chemcraft<sup>7</sup> or GaussView<sup>8</sup> softwares.

The quantum computational calculations were carried out in a cascading fashion, in case of geometry optimization, beginning from a primitive semi-empirical method followed by an *ab-initio* HF method and then to a density functional theory based on B3LYP method. This sequence can be easily understood from the representation, i.e., AM1 or PM3  $\rightarrow$  HF/STO-3G  $\rightarrow$  HF/3-21G  $\rightarrow$  HF/6-31G  $\rightarrow$  B3LYP/3-21G  $\rightarrow$  B3LYP/6-31G. Such a cascade methodology has been used throughout the present paper, unless otherwise mentioned. This is expected to minimize errors that may crop in if the crude model is directly taken to DFT methods, without going through this sequence of computations.

### Semi-empirical methods

The Austin Model 1 (AM1)<sup>9</sup> method was considered as the initial step for carrying out the computational modelling studies. The coordinates of the model generated or the one which is taken from the single crystal XRD structure are the first geometry minimised using this method. A full optimisation was carried out by using 'FOPT' keyword available without altering the default convergence criteria.

Parametric method 3 (PM3)<sup>10</sup> was used when the AM1 method did not give appreciable results. In most of the cases the PM3 method was used as the starting level of computational calculations and was used for full optimization procedure too.

### Ab initio method

Hartree-Fock (HF) level of theory was used for all the geometry optimization calculations.<sup>11</sup> This level of calculations was used for those models which were obtained from the semi-empirical calculations. The basis sets used in this are, STO-3G,<sup>12</sup> 3-21G<sup>13</sup> and 6-31G.<sup>14</sup>

### Density functional theory method

B3LYP method was used along with a set of basis sets, 3-21G, 6-31G with diffusion and polarisation functions involved wherever required. Also, ECP basis sets like CEP-121G,<sup>31</sup> SDD,<sup>15</sup> LanL2DZ<sup>15(a),16</sup> were used for the metal ions wherever required.

### Computational calculations

The initial guess structures used for computational calculations of **L**<sub>1</sub>, **L**<sub>2</sub>, **L**<sub>3</sub>, and **L**<sub>4</sub> were taken from the single crystal XRD data, whereas in the case of **L**<sub>5</sub>, the initial model was prepared from the published data of copper complex with the following modifications: (a) removing the copper center, (b) replacing *tert*-butyl moiety by hydrogen, (c) protonating the phenolate moieties, and, (d) introducing a -CH<sub>2</sub>OH moiety *ortho* to the phenolic OH of the Schiff base part of each of the arm. In order to reduce the computational times, cut short models of **L**<sub>1</sub>, **L**<sub>2</sub>, **L**<sub>3</sub> and **L**<sub>4</sub>, viz., **L**<sub>1</sub>' , **L**<sub>2</sub>' , **L**<sub>3</sub>' and **L**<sub>4</sub>' , were made by simply replacing each '*t*-butyl' group by 'H' and the benzimidazole by a simple imidazole moiety in the case of **L**<sub>1</sub>. Such modifications are not expected to affect either the conformation or the platform or the binding core to any significant extent and hence used in the computational calculations. Subsequently, the computations were carried out with the unmodified models also and no change was found in the conformation or in the binding core as demonstrated herein. The optimization of the metal complexes were carried out with the structures obtained at B3LYP/6-31G and deprotonated at both the phenolic centers of the Schiff base of the arms wherever required. The metal ion was placed well away from the binding core and allowed to minimize.

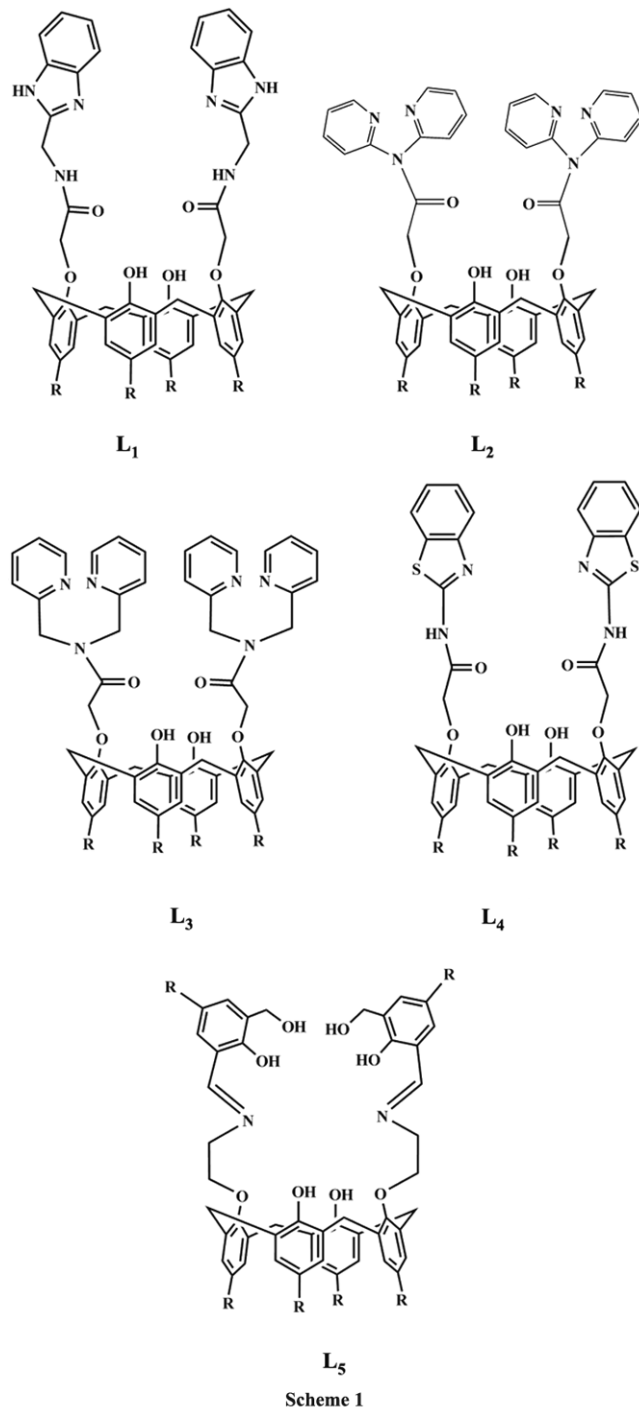
## Results and Discussion

During the past several years, our group has synthesized different 1,3-di-conjugates of calix[4]arene (Scheme 1) and demonstrated their selective recognition towards ions, viz., Ni<sup>2+</sup>, Cu<sup>2+</sup>, Zn<sup>2+</sup>, Ag<sup>+</sup>, Cd<sup>2+</sup> and Hg<sup>2+</sup> by using a variety of experimental methods. Since the formation of single crystals of the species of recognition has been the limiting step, structures of such complexes could not be established. However, the presence of crystal structure of either the receptor conjugate or its precursor was a boon to start the computational studies. Therefore, the structural features of the species of recognition of the complexes of the

conjugates of calix[4]arene have been presented based on computational methods carried out at the levels of DFT.

#### Reducing computational times

As can be seen from the Scheme 1, the conjugates of calix[4]arenes studied were all large in size with the total number of atoms ranging from ~150 to 200. All of these possess *t*-butyl moieties at their upper



rim, while the recognition or binding is through the binding groups present on the arms at the lower rim. Therefore, chopping of these four *t*-butyl groups will bring down the size of the conjugates to two-thirds of its original size. This indeed saves a lot of computational time without changing the conformational features of the arms which in turn provides the binding core. In order to keep the valency satisfied for the carbon center from which the corresponding *t*-butyl group was chopped off, the same was attached with hydrogen. Such a process yields not only a conformational invariant but also a molecule which is chemically intact. Hence, a number of computational calculations were carried out using such truncated conjugates of calix[4]arene as reported in this paper. All the receptor systems, viz., **L**<sub>1</sub>, **L**<sub>2</sub>, **L**<sub>3</sub>, **L**<sub>4</sub> and **L**<sub>5</sub> were subjected to this truncation and the resultant conjugates, viz., **L**<sub>1</sub>' , **L**<sub>2</sub>' , **L**<sub>3</sub>' , **L**<sub>4</sub>' and **L**<sub>5</sub>' were used for the computations. However, in the case of **L**<sub>1</sub>, an additional truncation was done by converting the benzimidazole to a simple imidazole moiety. Thus, all the truncations carried out on the original conjugate were balanced for their valencies by attaching the requisite number of H atoms. Some of the calculations were carried out with both the truncated as well as the original conjugate, and no significant change was found in the conformation of the arms as well as in the binding features. The cone conformation has been maintained throughout.

#### Cascade approach used in the computations

All the computations carried out and reported in this paper have been done through a cascade methodology. In this approach, a well optimized receptor geometry, which in turn is obtained from the crystal structure of the receptor, is taken initially in the semi-empirical methodology, and the outcome of this has been taken to the next higher level of calculations. Such computations are continued in a cascading manner by climbing to higher levels of calculations smoothly by going through AM1 or PM3 → HF/3-21G → HF/6-31G → B3LYP/3-21G → B3LYP/6-31G, etc. The metal ion is introduced in this cascade process at an appropriate stage and then the cascade taken further.

#### Hg<sup>2+</sup> recognition by **L**<sub>1</sub>

Based on our recent studies, **L**<sub>1</sub> has been found to be sensitive and selective in the recognition of Hg<sup>2+</sup> in aqueous acetonitrile (1:1) based on fluorescence spectroscopy.<sup>5h</sup> The stoichiometry of the complex

species formed during the titration was found to be 1:1 based on both the ESI MS and the absorption spectral studies. The selectivity of  $L_1$  towards  $Hg^{2+}$  has been demonstrated in comparison with eleven different and biologically relevant  $M^{2+}$  ions, viz.,  $Mn^{2+}$ ,  $Fe^{2+}$ ,  $Co^{2+}$ ,  $Ni^{2+}$ ,  $Cu^{2+}$ ,  $Zn^{2+}$ ,  $Cd^{2+}$ ,  $Hg^{2+}$ ,  $Pb^{2+}$ ,  $Ca^{2+}$  and  $Mg^{2+}$ , including those of the mercury group. None of these ions negatively influences the recognition of  $Hg^{2+}$  by  $L_1$ . The influence of solvent polarity on the recognition of  $Hg^{2+}$  has also been spectrally demonstrated. The species of recognition has been addressed by DFT computations as reported in this paper.

#### $L_1$ and $L_1'$

Both  $L_1$  and  $L_1'$  were optimized as explained in the methodology section and the corresponding structures obtained from B3LYP/6-31G are shown in Fig. 1. The optimized structures of  $L_1$  and  $L_1'$  exhibit almost similar changes in the dihedral angles (as shown in Fig. 1) of the arms when compared to that in  $L_1$  obtained from the single crystal XRD structure. The dihedral angles indeed confirmed the retainment of the arm-conformation on going from  $L_1$  to  $L_1'$ . The hydrogen bond present between the two imidazoles of the  $L_1$  was found to be intact even after the geometry optimization though minimal changes were observed in the metric data. The predicted hydrogen bond stabilization energy was obtained by mapping the energy from the H...A distance correlation plot reported in the literature.<sup>30</sup> It has been found that  $L_1$ (XRD),  $L_1$ (OPT) and  $L_1'$ (OPT) form a hydrogen bond with stabilization energies of -5.6, -4.6 and -5.3 kcal/mol respectively (where OPT refers to the optimized). The OPT geometries of both  $L_1$  and  $L_1'$  showed comparable changes in the dihedral angles, revealing minimal effect on crafting the system. The

ground state existence of the OPT geometries were checked by performing a vibrational state analysis and found that both the geometries had no imaginary frequencies.

#### $Hg^{2+}$ complex

The B3LYP/6-31G optimized geometries of  $L_1'$  and  $L_1$  were taken as the starting structures for modelling their  $Hg^{2+}$  complexes. The starting geometry was modelled by placing the  $Hg^{2+}$  ion away from the binding core of  $L_1/L_1'$  at a non-interacting distance, without disturbing the existing hydrogen bond. No attempt was made to deprotonate the imidazole proton of  $L_1$  or  $L_1'$  as the NMR spectra showed this proton intact. The geometry optimization of the modelled complex was carried out using B3LYP. The basis set used for  $Hg^{2+}$  was a compact effective potential basis set build by Stevens/Basch/Krauss, having a double and triple zeta, viz., CEP-31G followed by CEP-121G.<sup>31</sup> The trial computations with CEP-31G or CEP-4G prior to the usage of CEP-121G did not yield any favourable structures as mentioned in the literature.<sup>32</sup> The OPT structure of the  $Hg^{2+}$  complexes of  $L_1$  and  $L_1'$  are shown in Fig. 2. The ground state existence of the optimized geometry has been shown by performing vibrational state analysis.

The OPT  $HgL_1'/HgL_1$  complex showed the existence of a linear coordination around Hg with two of the imidazole nitrogens being bound, forming a species of the type  $N2...Hg...N5$  with an average  $Hg...N$  distance of  $\sim 2.09$  Å and  $N...Hg...N$  angle of  $178.6^\circ$  (Fig. 3(a&b)). Such linear coordination about  $Hg^{2+}$  is indeed common in the literature.<sup>33</sup> In addition to the interactions found with the imidazole N, a stabilizing interaction was observed between the  $Hg^{2+}$  and the two amide oxygens, wherein the  $Hg...O$  distance is  $\sim 2.7$  Å. Such stabilizing interactions

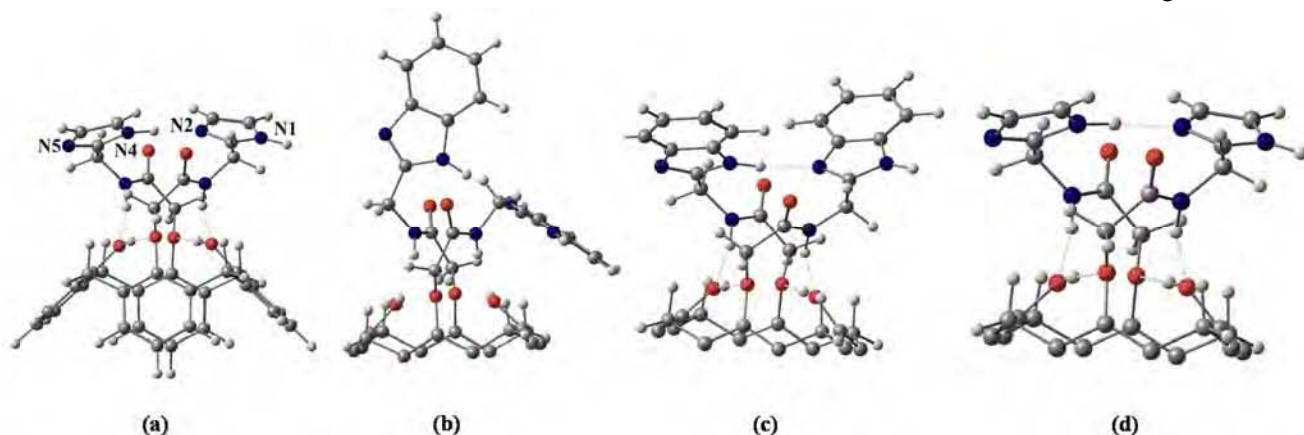


Fig. 1 – (a) B3LYP/6-31G optimized structures of  $L_1'$  and, (b) the arm portion of the lower-rim of  $L_1$  as obtained from single crystal XRD. B3LYP/6-31G optimized structures of  $L_1$  &  $L_1'$  are shown in (c) and (d) respectively.

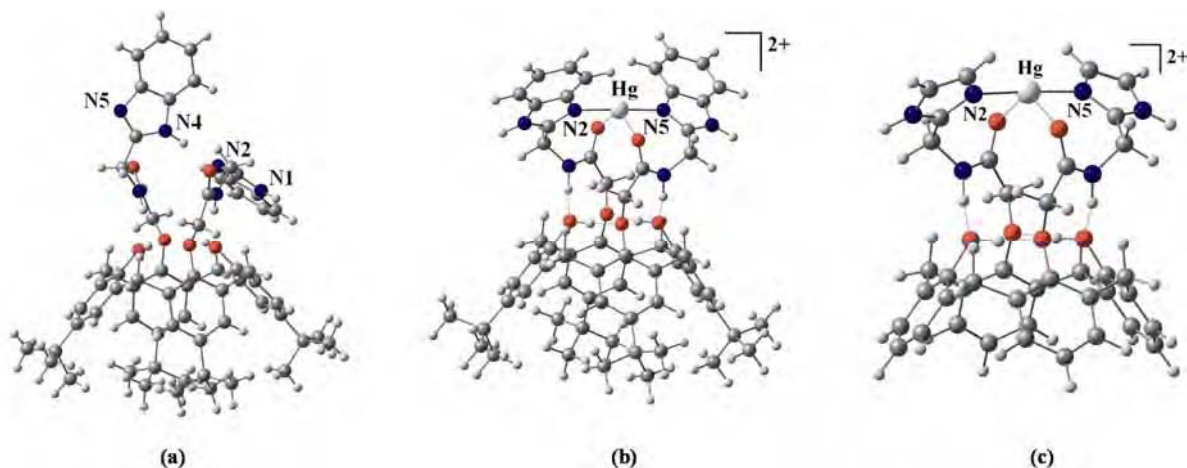


Fig. 2 – (a) Single crystal XRD structure of  $L_1$ . B3LYP/CEP-121G optimized structures of  $HgL_1$  and  $HgL_1'$  are given under (b) and (c) respectively.

were reported in the literature with different types of nitrogens in the range of 2.04 - 2.85 Å and oxygens in the range 2.57 - 2.95 Å.

The coordination complexes formed by  $L_1$  as well as  $L_1'$  with  $Hg^{2+}$  were almost the same, except for marginal variations in the metric data (shown in Fig. 3(a&b)). It has been reported in the literature that  $Hg^{2+}$  can exhibit interactions with groups or moieties other than N, O and S, viz., with aromatic rings, aliphatic groups, etc.<sup>34</sup> The overall coordination around Hg, viz., the two nitrogens and the two amide oxygens, resemble an octahedral geometry with two vacant sites as depicted in the Fig. 3(a&b).

#### Recognition of $Zn^{2+}$ and $Ni^{2+}$ by $L_2$

$L_2$  was found to selectively recognize  $Zn^{2+}$  (switch-on) and  $Ni^{2+}$  (switch-off) by showing changes in the fluorescence intensity by forming 1:1 complex.<sup>5c</sup> The binding studies of ions with  $L_2$  and the composition of the complex formed have been addressed by various experimental studies, viz., steady state and time resolved fluorescence spectroscopy, absorption spectroscopy and ESI MS. It was also found that  $L_2$  can detect  $Zn^{2+}$  and  $Ni^{2+}$  to a minimum concentration of 142 and 203 ppb respectively, making  $L_2$  an efficient molecular probe for these ions.  $L_2$  has also been experimentally found to recognize both these metal ions simultaneously in a cooperative manner, viz.,  $Ni^{2+}$  and  $Zn^{2+}$ . The experimentally observed fluorescence intensity of the complex  $[ZnL_2]$  decreases when titrated against  $Ni^{2+}$  and increases when  $[NiL_2]$  was titrated against  $Zn^{2+}$ . These results clearly suggest the cooperative binding of  $Zn^{2+}$  and  $Ni^{2+}$  to  $L_2$ , immaterial of whether the  $L_2$  was initially loaded with  $Zn^{2+}$  or with  $Ni^{2+}$ .

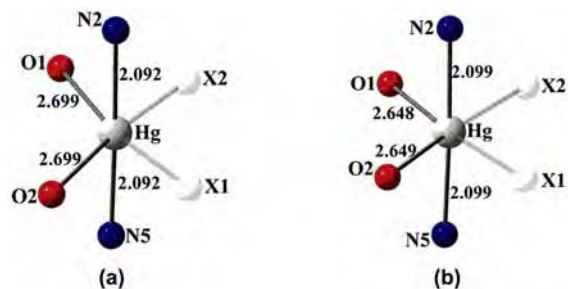


Fig. 3 – The coordination sphere of  $Hg^{2+}$  present in (a)  $HgL_1$ , and, (b)  $HgL_1'$  as obtained from B3LYP/CEP-121G optimization calculations. [The coordination spheres of  $HgL_1$  and (b)  $HgL_1'$  exhibit the following bond angles ( $^\circ$ ):  $N2-Hg-O1 = 95.2/96.0$ ;  $N2-Hg-O2 = 84.2/83.2$ ;  $N2-Hg-N5 = 178.6/177.9$ ;  $O1-Hg-O2 = 135.4/131.2$ ;  $O1-Hg-N5 = 84.3/83.2$  and  $O1-Hg-N5 = 95.3/96.0$ .  $X1=X2=$  vacant site].

Thus, the mononuclear (viz.,  $Ni^{2+}$  or  $Zn^{2+}$ ) and the dinuclear (viz., both  $Ni^{2+}$  and  $Zn^{2+}$ ) species of recognition were modelled by DFT calculations.

#### $L_2$ and $L_2'$

Geometry optimization on both  $L_2$  and  $L_2'$  were carried out as mentioned under methodology and the structures of DFT (B3LYP with 6-31G basis set) optimized  $L_2$  and  $L_2'$  are shown in Fig. 4. The optimization of  $L_2$  and  $L_2'$  resulted in similar structures and are different from that of the crystal structure. The ground state existence of the OPT geometries of both  $L_2$  and  $L_2'$  were checked by performing a vibrational state analysis. When arm-to-arm dihedral angle comparison was made (Fig. 4), it was found that the dihedral angles were very similar among both the optimized structures ( $L_2$  and  $L_2'$ ), though these were considerably different from that observed in the crystal structure. The orientation of the pyridyl groups present in the single crystal structure undergoes appreciable changes upon

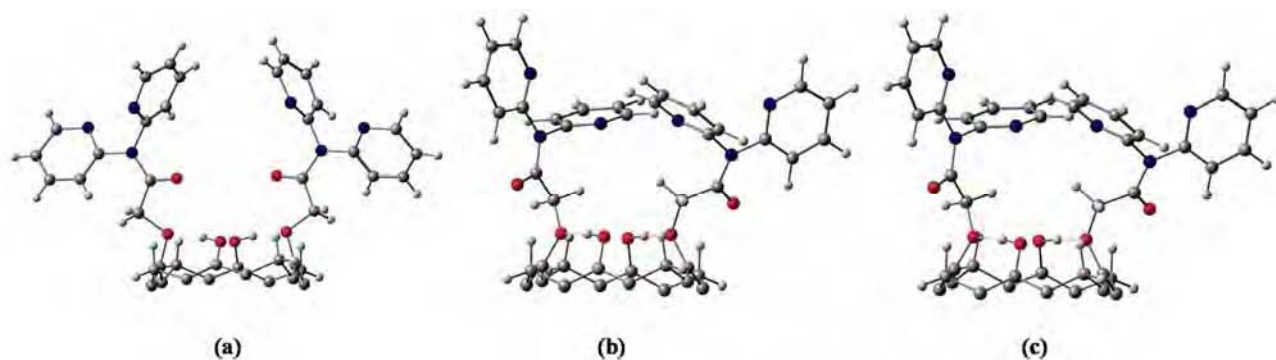


Fig. 4 – (a) The arm portion of the lower-rim of  $L_2$  as obtained from single crystal XRD. B3LYP/6-31G optimized structures of  $L_2$  and  $L_2'$  are shown in (b) and (c) respectively.

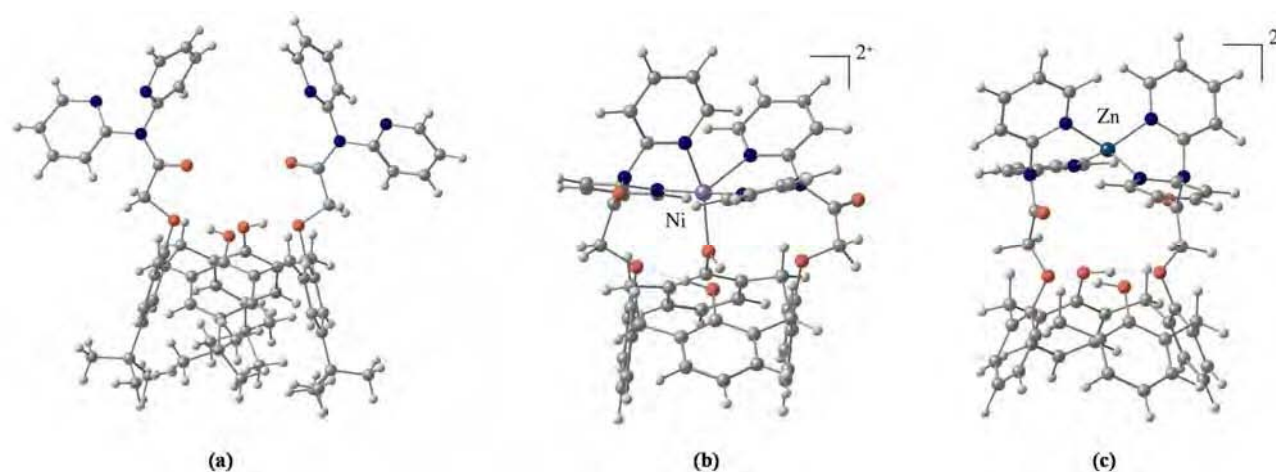


Fig. 5 – (a) Single crystal XRD structure of  $L_2$ . B3LYP/6-31G\* optimized structures of  $[NiL_2']^{2+}$  and  $[ZnL_2']^{2+}$  are given under (b) and (c) respectively.

optimisation to bring the nitrogens in a position that is favourable for the metal ion binding. The formation of favourable metal ion binding core can be quantified by the decrease observed in the inter arm N...N distances, viz., from 6.45–11.48 Å (XRD) to 3.46 – 8.96 Å (optimized structure).

#### Mononuclear $Ni^{2+}$ or $Zn^{2+}$ complex of $L_2'$

The  $L_2'$  that was obtained from DFT calculations was taken as the initial structure for the computational modelling of the complexes. The model for the complex was generated by placing either  $Ni^{2+}$  or  $Zn^{2+}$  at a non-interacting position well above the pyridyl core of the  $L_2'$  and maintaining the overall charge on the complex to be +2. The computational calculations were carried out for both the  $[NiL_2']^{2+}$  and  $[ZnL_2']^{2+}$  complexes at B3LYP/6-31G(d) level. The optimized structures of these complexes are shown in Fig. 5(b&c) respectively. The complexation in the case of  $L_2'$  is a result of the metal ion induced conformational changes brought about in the pendant arms of  $L_2'$  so that the core possessing the ligating atoms is well poised for binding.

In case of  $[NiL_2']^{2+}$  complex, the  $Ni^{2+}$  exhibited a distorted octahedral geometry with one of the coordination sites being vacant by forming covalent bonds with all the four pyridyl nitrogens along with one weak bond being formed with one of the lower rim phenolic-OH (Fig. 5b). The distortion in the  $Ni^{2+}$  geometry can be clearly gauged from the angles observed in the coordination sphere, viz., 83 - 115° (as compared to 90°) and 155 - 160° (as compared to 180°) (Fig. 6a). A literature report<sup>35</sup> shows the Ni-N distance to be 1.84 - 2.05 Å or more, which is similar to that found in the present case, viz., 1.91 - 2.42 Å.

In the case of  $[ZnL_2']^{2+}$ , the  $Zn^{2+}$  exhibits a distorted tetrahedral geometry by binding through all the four pyridyl nitrogens (Fig. 5c), similar to that found in the case of  $Ni^{2+}$  complex but in a tetrahedral geometry. The angles observed in the coordination sphere, viz., 95 - 134°, clearly suggests a considerable distortion in the tetrahedral geometry (Fig. 6b). It has been reported in the literature that the Zn...N distances<sup>36</sup> are in the range of 2.03 - 2.48 Å.

### Hetero-binuclear complex of $[Zn-L_2''-Ni]^{4+}$

Based on the experimental results of simultaneous recognition of  $Ni^{2+}$  and  $Zn^{2+}$  by  $L_2$  in a cooperative fashion, an attempt to model a hetero-bimetallic complex of this conjugate was initiated. Geometry optimization studies in the presence of both the cations was carried out with the optimized  $Zn^{2+}$  complex of  $L_2'$  followed by placing  $Ni^{2+}$  at a non-interacting position above  $Zn^{2+}$ . To reduce the computational time required for these calculations further,  $L_2''$  was derived from  $L_2'$ , by replacing the phenyl rings of the calixarene by hydrogens, taking care of the hybridization at each center appropriately. The optimizations resulted in the formation of a new complex. In this new complex, while the  $Ni^{2+}$  occupies the  $N_4$  core of the pyridyls, that of the  $Zn^{2+}$  has been pushed to the O-rich core of the lower rim by forming a distorted trigonal bipyramidal geometry (Fig. 7). The  $Ni...N$  and  $Zn...O$  bond distances were found to be in the range of 1.90 - 2.11 Å, which is similar to that reported in the literature.<sup>35,36</sup>

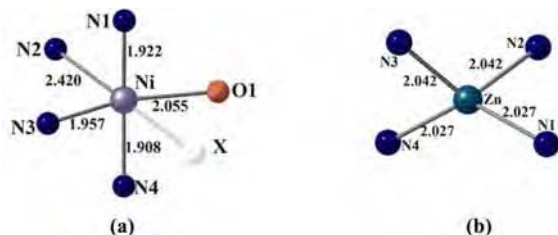


Fig. 6 – The coordination spheres of (a)  $Ni^{2+}$  in  $[NiL_2']^{2+}$  and (b)  $Zn^{2+}$  in  $[ZnL_2']^{2+}$  as obtained from B3LYP/6-31G\* optimization calculations. [X = vacant site. The bond angles ( $^\circ$ ) around  $Ni^{2+}$  in the coordination sphere are: N1-Ni-N2 = 88.4, N1-Ni-N3 = 86.8, N1-Ni-N4 = 168.7, N1-Ni-O1 = 94.0, N2-Ni-N3 = 90.3, N2-Ni-N4 = 100.9, N2-Ni-O1 = 109.1, N3-Ni-N4 = 86.9, N3-Ni-O1 = 160.7, N4-Ni-O1 = 88.9, N1-Zn-N2 = 96.2, N1-Zn-N3 = 106.3, N1-Zn-N4 = 133.5, N2-Zn-N3 = 120.8, N2-Zn-N4 = 106.3, N3-Zn-N4 = 96.2].

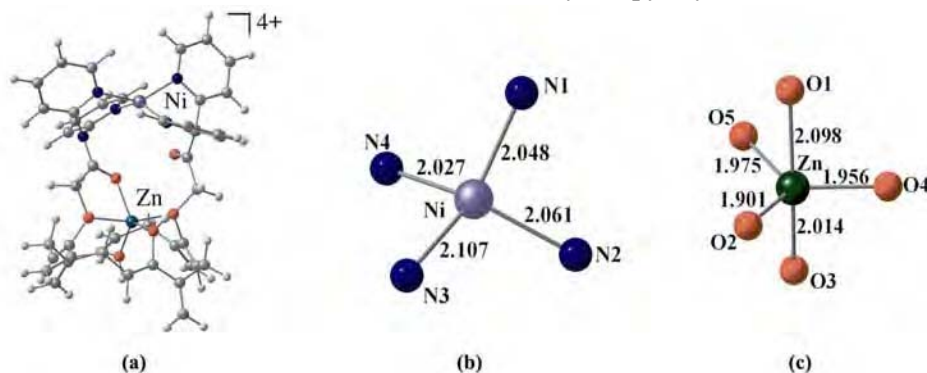


Fig. 7 – (a) HF/3-21G optimized structure of  $[Zn-L_2''-Ni]^{4+}$  complex. The coordination spheres of (b)  $Ni^{2+}$  and (c)  $Zn^{2+}$  as obtained from HF/3-21G optimised complex of  $[Zn-L_2''-Ni]^{4+}$ . [The bond angles ( $^\circ$ ) around  $Ni^{2+}$  and  $Zn^{2+}$  in the coordination sphere are: N1-Ni-N2 = 93.1, N1-Ni-N3 = 140.7, N1-Ni-N4 = 97.1, N2-Ni-N3 = 100.8, N2-Ni-N4 = 145.0, N3-Ni-N4 = 92.2, O1-Zn-O2 = 95.1, O1-Zn-O3 = 166.0, O1-Zn-O4 = 90.4, O1-Zn-O5 = 73.9, O2-Zn-O3 = 96.7, O2-Zn-O4 = 118.0, O2-Zn-O5 = 119.1, O3-Zn-O4 = 90.8, O3-Zn-O5 = 93.7, O4-Zn-O5 = 121.6].

The geometry optimization calculations resulted in the conformational changes at the arms since two binding cores are observed and the deviation of the conformation with respect to that present in the crystal structure of  $L_2$  are rather substantial. The conformational changes are gauged by the changes observed in the dihedral angles of the arms.

### $Cu^{2+}$ and $Ag^+$ recognition by $L_3$

$L_3$  was studied for its metal ion binding properties towards various biologically relevant  $M^{n+}$  transition/alkali/alkaline earth ions by fluorescence and absorption spectroscopy in two different solvent systems.  $L_3$  was found to detect  $Cu^{2+}$  (switch-on fluorescence at 315 nm) and  $Ag^+$  (ratiometrically switch-on fluorescence at 445 nm) selectively in pure and aqueous methanol media.<sup>5f,5g</sup> The stoichiometry of the copper or the silver complex has been found to be 1:1, based on the Job's plot and was further confirmed by ESI-MS. The corresponding  $Ag^+$  and  $Cu^{2+}$  complexes were modelled by computational studies as reported here.

### $L_3$ and $L_3'$

Both  $L_3$  and  $L_3'$  were geometry optimized as given under Methodology and the corresponding structures are shown in Fig. 8. The geometry optimization of the  $L_3$  and  $L_3'$  showed similar orientation of the arms, but both showed appreciable changes in the dihedral angles at the arms when compared to the angles present in the crystal structure. The distance between the pyridyl nitrogens in the intra arms as well as the inter arm of  $L_3$  were found to change from 4.88 – 5.39 Å (with an average of 3.73 Å) in the case of intra arm, and 5.09 – 8.87 Å to 4.66 – 5.50 Å in the case of inter arms, upon optimization. The data clearly suggest the formation of a favourable binding core by the pyridyl moieties for metal ion by bringing

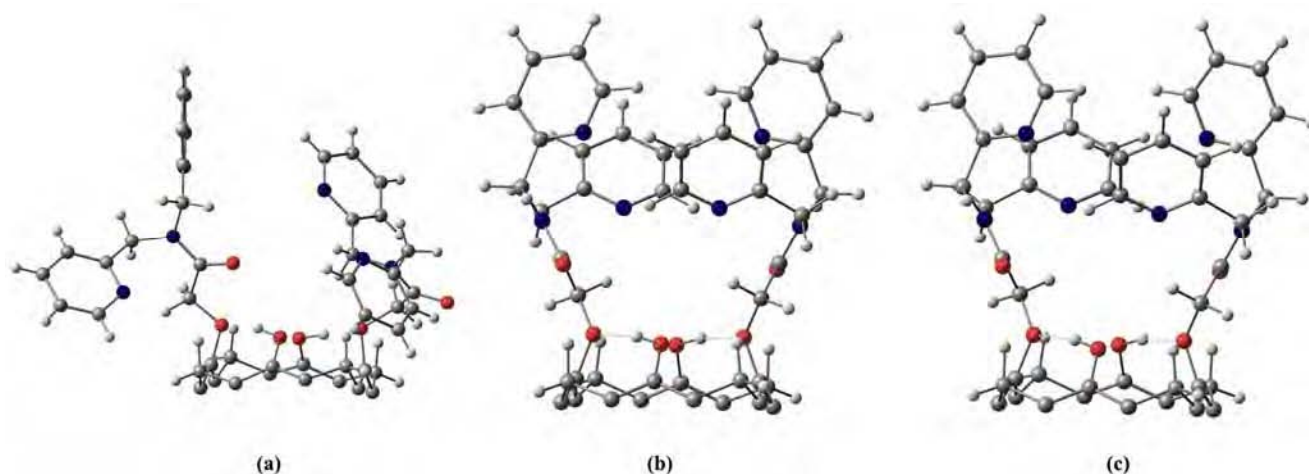


Fig. 8 – (a) The arm portion of the lower-rim of  $L_3$  as obtained from single crystal XRD. B3LYP/6-31G optimized structures of  $L_3$  and  $L_3'$  are shown in (b) and (c) respectively.

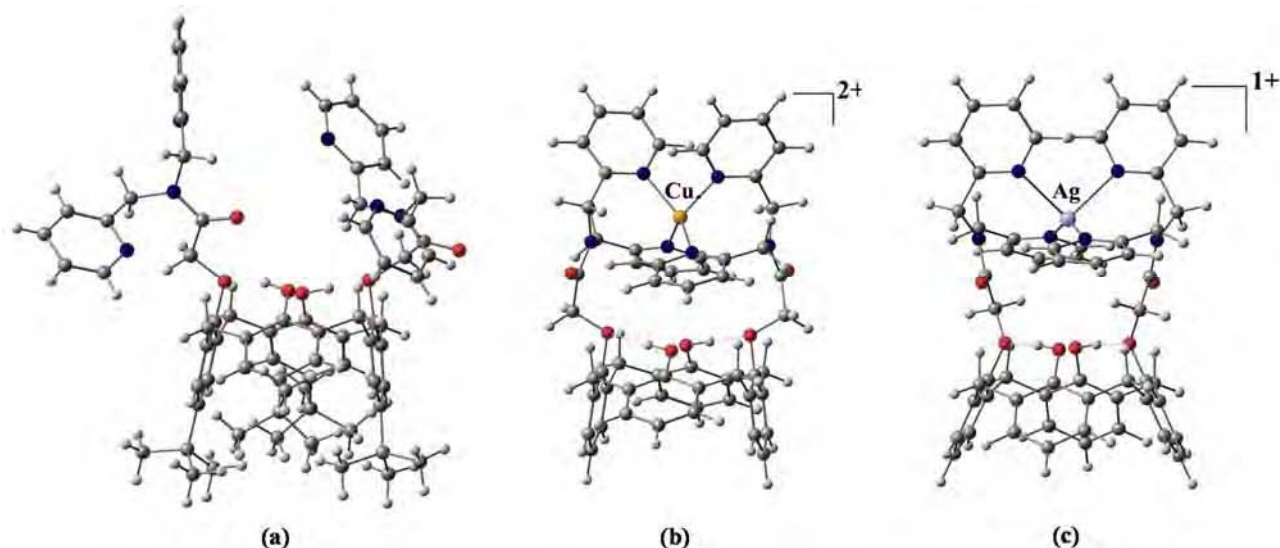


Fig. 9 – (a) Single crystal XRD structure of  $L_3$ , (b) B3LYP/6-31G\* optimised structure of the copper complex  $[CuL_3']^{2+}$ , and (c) B3LYP/SDD optimised structure of the silver complex  $[AgL_3']^+$ .

the nitrogen centers of these into a coordinating distance. The variations occurred in the conformation of the arms of  $L_3/L_3'$  as compared to the single crystal structure as can be seen from the Fig. 8.

#### $Cu^{2+}$ or $Ag^+$ complex of $L_3'$

The DFT optimized geometry of  $L_3'$  was taken as the initial structure for generating models for the copper and silver complexes. The model was generated by placing the  $Cu^{2+}$  or  $Ag^+$  at a non-interacting distance, well above the pyridyl-nitrogen core of  $L_3'$ . The models were then geometry optimized to the highest level of B3LYP with 6-31G basis set in the case of copper complex and SDD basis set in the case of silver complex. The overall charge of the complexes were maintained as  $[CuL_3']^{2+}$

and  $[AgL_3']^+$  respectively. The OPT structures of these complexes are shown in Fig. 9(b&c) respectively for  $[CuL_3']^{2+}$  and  $[AgL_3']^+$ .

In the case of  $[CuL_3']^{2+}$  complex, the  $Cu^{2+}$  site exhibits a distorted tetrahedral geometry extending its four coordinations to four of the pyridyl nitrogens present. The distortion in the geometry can be measured from the coordination angles observed at the copper center, viz.,  $89.3 - 141.8^\circ$  (as compared to  $109^\circ 7'$ ). The coordination bond lengths and bond angles are given in the caption of Fig. 10. Such a highly distorted tetrahedral center was observed for  $Cu^{2+}$  in blue copper proteins, viz., plastocyanin.<sup>37</sup> In case of the protein, the presence of such distorted copper center has been interpreted to its ease

to undergo redox process during the electron transfer activity. Comparable geometric parameters have also been observed in the literature about a copper center.<sup>38</sup>

In the case of  $[\text{AgL}_3']^+$  complex,  $\text{Ag}^+$  also exhibits a distorted tetrahedral geometry, extending its four coordination through the four pyridyl nitrogens. The extent of distortion present in the  $[\text{AgL}_3']^+$  complex is almost comparable to that of the copper complex  $[\text{CuL}_3']^{2+}$  (Fig. 11). Similar coordination geometry has been found in the literature.<sup>39</sup>

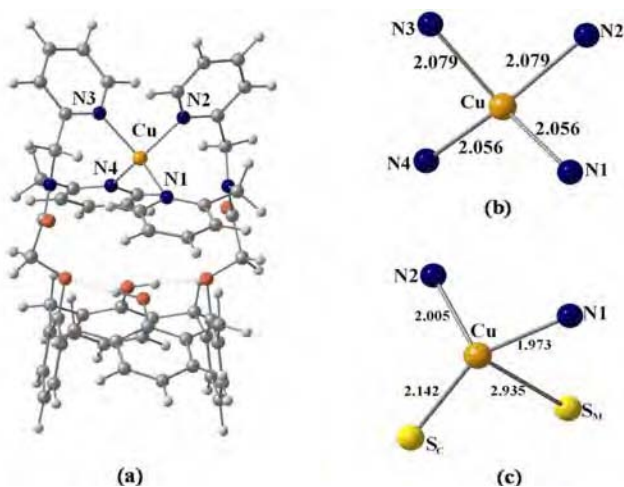


Fig. 10 – (a) B3LYP/6-31G\* optimized structure of  $[\text{CuL}_3']^{2+}$ . The coordination sphere of  $\text{Cu}^{2+}$  present in (b)  $[\text{CuL}_3']^{2+}$  and (c) plastocyanin (PDB id: 1BXU). [The bond angles ( $^\circ$ ) around  $\text{Cu}^{2+}$  in the coordination sphere of  $[\text{CuL}_3']^{2+}$  and plastocyanin are:  $\text{N1} - \text{Cu} - \text{N2} = 90.5$ ,  $\text{N1} - \text{Cu} - \text{N3} = 141.8$ ,  $\text{N1} - \text{Cu} - \text{N4} = 112.1$ ,  $\text{N2} - \text{Cu} - \text{N3} = 89.3$ ,  $\text{N2} - \text{Cu} - \text{N4} = 141.8$ ,  $\text{N3} - \text{Cu} - \text{N4} = 90.5$  and  $\text{N1} - \text{Cu} - \text{N2} = 101.4$ ,  $\text{N1} - \text{Cu} - \text{S}_M = 98.8$ ,  $\text{N1} - \text{Cu} - \text{S}_C = 121.4$ ,  $\text{N2} - \text{Cu} - \text{S}_M = 86.0$ ,  $\text{N2} - \text{Cu} - \text{S}_C = 131.0$ ,  $\text{S}_M - \text{Cu} - \text{S}_C = 107.7$  respectively].

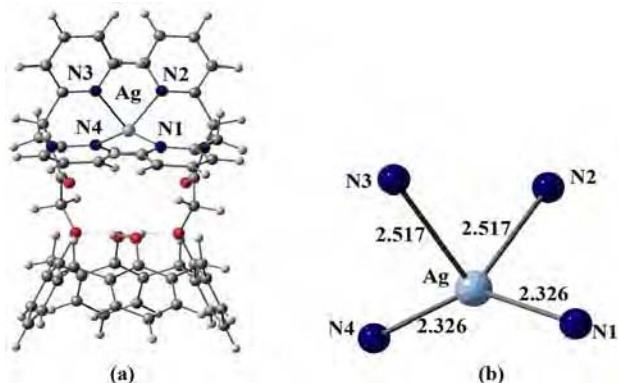


Fig. 11 – (a) B3LYP/SDD optimized structure of  $[\text{AgL}_3']^+$ . (b)  $\text{Ag}^+$  coordination sphere of  $[\text{AgL}_3']^+$ . [The coordination angles ( $^\circ$ ) around  $\text{Ag}^+$  are:  $\text{N1} - \text{Ag} - \text{N2} = 109.7$ ;  $\text{N1} - \text{Ag} - \text{N3} = 91.8$ ;  $\text{N1} - \text{Ag} - \text{N4} = 147.1$ ;  $\text{N2} - \text{Ag} - \text{N3} = 98.9$ ;  $\text{N2} - \text{Ag} - \text{N4} = 91.8$  and  $\text{N3} - \text{Ag} - \text{N4} = 109.7$ ].

#### Recognition of $\text{Cu}^{2+}$ by $\text{L}_4$

The receptor molecule,  $\text{L}_4$  exhibited selectively the fluorescence quenching towards  $\text{Cu}^{2+}$  alone among the eleven divalent ions studied.<sup>5d</sup> The 1:1 stoichiometry of the complex formed between  $\text{L}_4$  and  $\text{Cu}^{2+}$  has been demonstrated by electronic absorption and ESI-MS. The structural features of the  $\text{Cu}^{2+}$  complex of  $\text{L}_4$  have been established by DFT.

#### Optimization of $\text{L}_4'$

$\text{L}_4'$  was optimized as explained earlier and the corresponding structure obtained from HF/3-21G calculation is shown in Fig. 12. The optimized structure of  $\text{L}_4'$  exhibits no significant change in the dihedral angles of the arms as compared to the single crystal XRD structure of  $\text{L}_4$ . The hydrogen bond present between the lower rim phenolic core of the  $\text{L}_4'$  was found to be intact even after the geometry optimization. The optimized geometry of  $\text{L}_4'$  showed no comparable changes in the dihedral angles of the arms as compared to that of the single crystal X-ray structure of  $\text{L}_4$ , revealing minimal or no effect on replacing the *t*-butyl groups by hydrogen atoms.

#### $\text{Cu}^{2+}$ complex of $\text{L}_4'$

The B3LYP/6-31G optimized structure of  $\text{L}_4'$  was taken as the starting structure for modeling the  $\text{Cu}^{2+}$  complex. The optimization of the complex was carried out by simply placing the  $\text{Cu}^{2+}$  far above the binding core so that initially there are no interactions between  $\text{L}_4'$  and  $\text{Cu}^{2+}$ . The minimization of the modeled complex was carried out using B3LYP/6-31G\*. The optimization resulted in a four coordinated distorted trigonal bipyramidal  $\text{Cu}(\text{II})$  complex with one vacant site. The resultant structure was further allowed to fill the vacant coordination by an acetonitrile. The optimization carried out in the

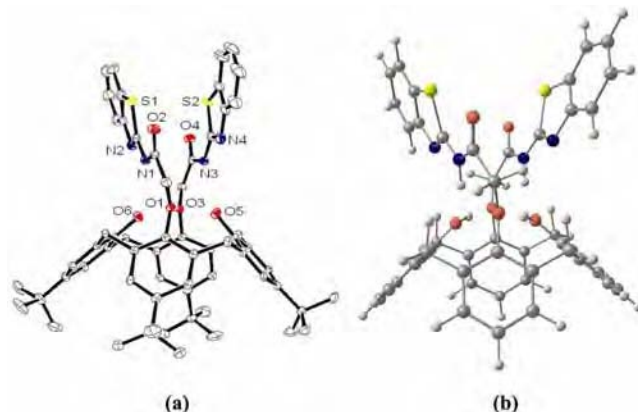


Fig. 12 – (a) Single crystal x-ray structure of  $\text{L}_4$ , and, (b) HF/3-21G optimized structure of  $\text{L}_4'$ .

presence of acetonitrile in B3LYP/6-31G\* resulted in a complex where  $\text{Cu}^{2+}$  exhibits a distorted trigonal bipyramidal geometry wherein each arm of  $\text{L}_4'$  acts as bidentate in providing a total of four coordinations, with the fifth coordination coming from the acetonitrile, resulting in  $\text{NO}_2\text{S}_2$  binding core (Fig. 13(a&b)). Similar coordination geometry and bond distances were observed for a Cu(II) complex of 1,6-bis(2-benzimidazolyl)-2,5-dithiahexane.<sup>40</sup>

#### Differential recognition of $\text{Zn}^{2+}$ over $\text{Cd}^{2+}$ by $\text{L}_5$

$\text{L}_5$  showed selectivity toward  $\text{Zn}^{2+}$  by switch-on fluorescence among the 12 metal ions studied.<sup>5c</sup> The interaction of  $\text{Zn}^{2+}$  with  $\text{L}_5$  has been further supported by absorption studies, and the stoichiometry of the complex formed (1:1) has been established on the basis of the absorption and ESI MS. The receptor also showed fluorescence enhancement with  $\text{Cd}^{2+}$  but this is much less than that exhibited by  $\text{Zn}^{2+}$ . The differential recognition of  $\text{L}_5$  towards  $\text{Zn}^{2+}$  over  $\text{Cd}^{2+}$  has been computationally established.

$\text{L}_5'$  was optimized as before and the structure obtained from B3LYP/6-31G is shown in Fig. 14. The OPT structure observed at B3LYP/6-31G level of calculations showed well ordered arms in an extended fashion wherein each arm is stabilized through phenolic O-H...N hydrogen bond interaction (intra-arm). In addition, one of the arms extends a weak hydrogen bond, viz., alcoholic O-H...O

(phenolic). Further, the two arms are connected through a hydrogen bond formed between their alcoholic-OH groups (inter arm), as can be seen from Table 1. The hydrogen-bond interactions observed at the phenolic lower rim indicates cone conformation; the inter arm interactions also supports the conformation.

#### $\text{Zn}^{2+}$ complex of $\text{L}_5'$

To obtain the  $\text{Zn}^{2+}$  complex, the structure of  $\text{L}_5'$  obtained at B3LYP/6-31G level was deprotonated at both the phenolic centers of the Schiff base of the arms to form deprotonated  $\text{L}_5'$ . The metal ion was placed well above the arms of the deprotonated  $\text{L}_5'$  and allowed to minimize. The minimization in the presence of metal ion was carried out in a cascade fashion starting from PM3  $\rightarrow$  HF/STO-3G  $\rightarrow$  HF/3-21G  $\rightarrow$  HF/6-31G  $\rightarrow$  B3LYP/3-21G  $\rightarrow$  B3LYP/6-31G  $\rightarrow$  B3LYP/LanL2DZ. Such minimizations resulted in formation of the  $\text{Zn}^{2+}$  complex by breaking the hydrogen-bond interactions present between the two arms. The  $\text{Zn}^{2+}$  interacts primarily at the Schiff base core (Fig. 15) and showed distorted four-coordination geometry bonded through two imine nitrogens and two Schiff base phenolate

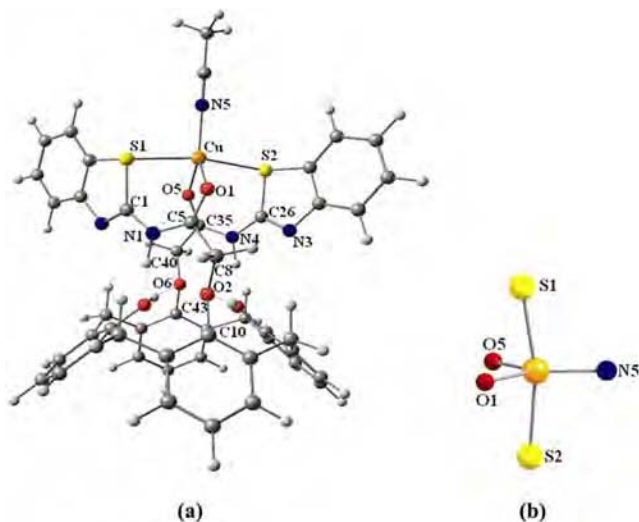


Fig. 13 – (a) B3LYP/6-31G\* optimized structure of  $[\text{CuL}_4']^{2+}$ , and (b) coordination geometry around  $\text{Cu}^{2+}$ . [The bond distances (Å) and bond angles (°) around  $\text{Cu}^{2+}$  in the coordination sphere are: Cu-N5 = 1.922, Cu-S1 = 2.493, Cu-S2 = 2.522, Cu-O1 = 2.139 and Cu-O5 = 2.095 Å; and S1-Cu-S2 = 168.2, N5-Cu-O1 = 124.1, N5-Cu-O5 = 128.5, O1-Cu-O5 = 107.4, S1-Cu-N5 = 96.2, S1-Cu-O1 = 77.3, S1-Cu-O5 = 95.2, S2-Cu-N5 = 95.5, S2-Cu-O1 = 95.5, S2-Cu-O5 = 77.9 ].

Table 1 – Hydrogen bond data for  $\text{L}_5'$

Hydrogen bond	H...A (Å)	D...A (Å)	D-H...A (°)
O6-H30...N2	1.479	2.467	150.0
O8-H46...O6	1.828	2.641	137.3
O7-H41...O8	1.759	2.738	167.5
O4-H13...N1	1.618	2.545	147.7

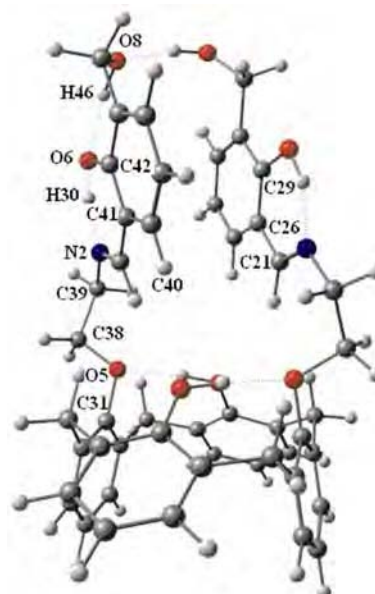


Fig. 14 – B3LYP/6-31G-optimized structure of  $\text{L}_5'$  stabilized through both the intra- and inter-arm hydrogen bonds.

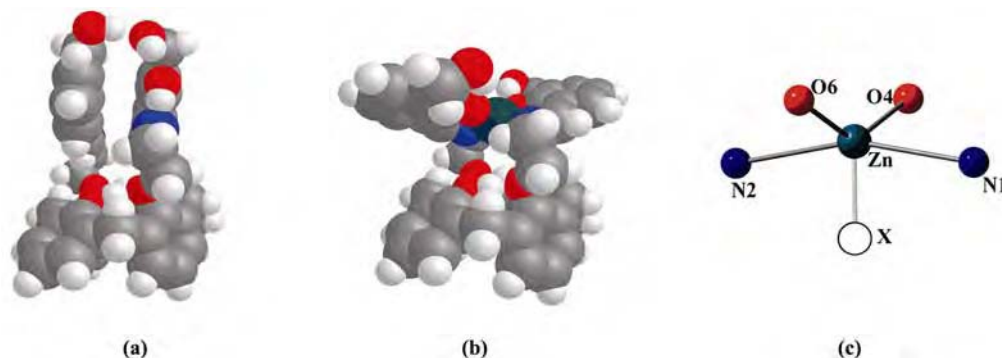


Fig. 15 – Space filling models of (a) B3LYP/6-31G optimized structure of  $L_5'$ , (b) B3LYP/LanL2DZ optimized structure of  $[ZnL_5']$ , and, (c) coordination core of  $[ZnL_5']$ . [The unfilled circle 'X' represents vacant site. The metric data for  $[ZnL_5']$ : N1-Zn = 2.071, N2-Zn = 2.072, O6-Zn = 1.979 and O4-Zn = 1.979 Å; N2-Zn-N1 = 161.7, N2-Zn-O6 = 91.3, N2-Zn-O4 = 94.8, N1-Zn-O6 = 94.8, N1-Zn-O4 = 91.3 and O6-Zn-O4 = 141.5].

oxygens. The Zn-O and Zn-N distances were found to be 1.979 and 2.072 Å, respectively, which are found commonly in the literature. The coordination angles observed with the  $Zn^{2+}$  core provides a better fit if it were to be considered as a trigonal bipyramidal with one trigonal center being vacant, where the *trans*-angle<sup>41</sup>, viz., N1-Zn-N2, is found to be 162°.

#### $Cd^{2+}$ complex of $L_5'$

The optimization of  $Cd^{2+}$  complex of  $L_5'$  was carried out with the structure of  $L_5'$  obtained at B3LYP/6-31G deprotonated at its both the phenolic centers of the Schiff base of the arms. The metal ion was placed well above the arms of the deprotonated  $L_5'$  and allowed to minimize. The minimization in the presence of the metal ion was carried out in a cascade fashion starting from HF/STO-3G  $\rightarrow$  HF/3-21G  $\rightarrow$  B3LYP/3-21G  $\rightarrow$  B3LYP/LanL2DZ. Such minimizations resulted in the formation of  $Cd^{2+}$  complex by breaking the hydrogen-bond interactions present between the two arms. The  $Cd^{2+}$  primarily interacts at the lower rim phenolic core and shows a distorted six coordination geometry bonded through two imine nitrogens, two Schiff base phenolic oxygens, and two lower rim phenolic groups (Fig. 16). The Cd-O and Cd-N distances were found to be 2.229-2.445 and 2.323-2.377 Å, respectively and are in agreement with what is commonly found in the literature.<sup>42</sup> The coordination angles observed with the  $Cd^{2+}$  core provide a better fit if it were to be considered as a seven-coordinated capped octahedral structure with one vacant site.

#### Conclusions and Correlations

The experimentally observed species of recognition has been computationally modelled in a cascade fashion from semi empirical to DFT level, via, several

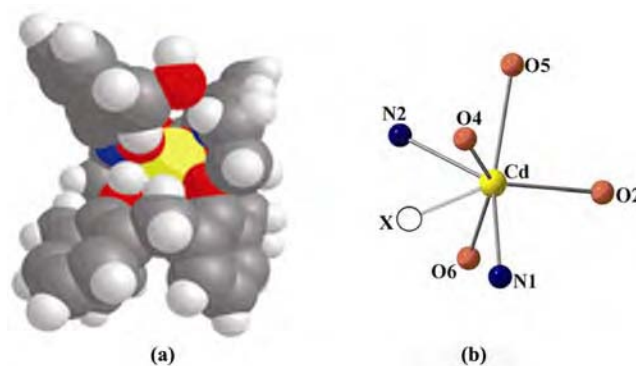


Fig. 16 – (a) Space filling model of B3LYP/LanL2DZ optimized structure of  $[CdL_5']$ , and, (b) coordination core of  $[CdL_5']^{2+}$ . [The unfilled circle 'X' represents vacant site. The metric data for  $[CdL_5']^{2+}$ : N1-Cd = 2.377, N2-Cd=2.323, O2-Cd = 2.445, O4-Cd = 2.325, O5-Cd=2.441 and O6-Cd = 2.229 Å; N1-Cd-O5 = 147.4, N1-Cd-O2 = 98.5, N1-Cd-O4 = 76.8, N1-Cd-N2 = 129.2, N1-Cd-O6 = 84.6, O2-Cd-O5 = 82.7, N2-Cd-O2 = 125.5, N2-Cd-O4 = 91.0, N2-Cd-O5 = 70.6, N2-Cd-O6 = 79.1, O2-Cd-O6 = 81.2, O2-Cd-O4 = 128.9, O4-Cd-O5 = 77.3, O4-Cd-O6 = 146.2 and O5-Cd-O6 = 127.4].

stages of calculations. These are done with six different ions using five different conjugates of calix[4]arene. Important features of the species of recognition are given in Fig. 17 for appropriate comparison for all these cases. Since the coordinating atoms and geometry of the metal center are important for the recognition process, all such features can be seen on a comparative basis from this figure. As can be seen from Fig. 17, the binding cores vary from  $N_2$  to  $N_4$  to  $N_4OX$ ,  $N_2O_2X_2$ ,  $O_5$ ,  $N_2O_2$  to  $NO_2S_2$ ,  $N_2O_2X$ ,  $N_2O_4X$ ,  $NO_4$  (X = vacant coordination site), while the geometries vary from linear to distorted tetrahedron ( $T_d$ ) to a situation that is in between distorted tetrahedron and distorted square planar (SP) to distorted trigonal bipyramid (TBP) to distorted octahedral ( $O_h$ ) with vacant site(s), distorted square

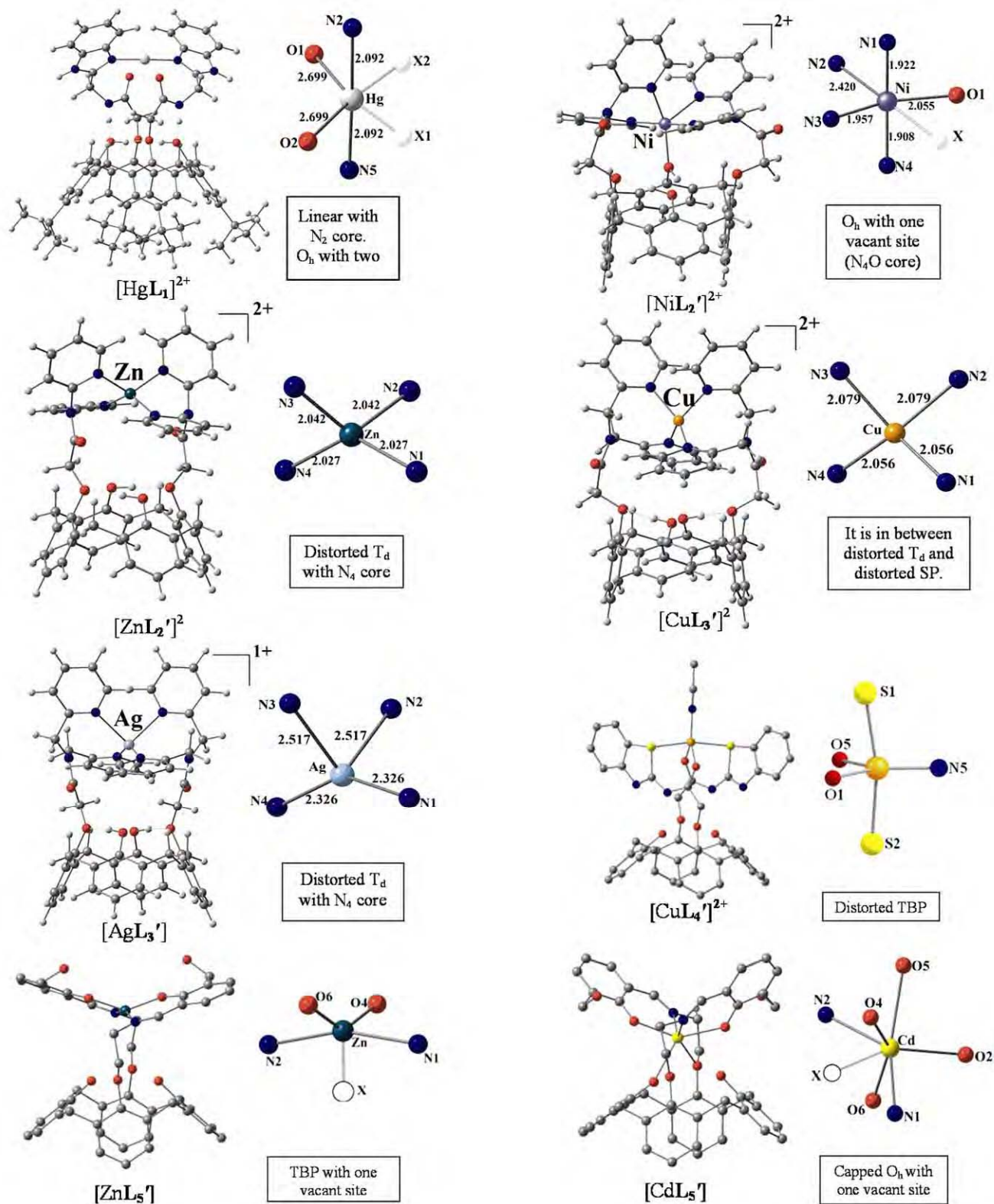


Fig. 17 – Species of ion recognition of calix[4]arene conjugates. [O<sub>h</sub> = octahedral; T<sub>d</sub> = tetrahedral; TBP = trigonal bipyramidal; SP = square planar].

pyramidal to distorted octahedral ( $O_h$ ) to capped octahedral with one vacant site. Thus, a large variation is found both in the binding core as well as in the geometry, and hence, the arms are able to sense ions with diverse coordination preferences.

Most of these geometries were found to be distorted owing to their wide range of angles in the coordination sphere. Indeed several metal ion cores present in metalloproteins also possesses highly distorted geometries, since such distortions favour the function and/or reactivity. A vivid example of this is the Cu(II) center present in plastocyanin; the geometry observed in the copper complex of  $L_3$  is very similar to that observed in plastocyanin. Therefore, the distorted geometries observed based on the present computational studies (Fig. 17) may very well support the geometries observed at the metal centers of metalloproteins.

While the  $Hg^{2+}$  complex of  $L_1$  exhibits a perfectly linear geometry as N-Hg-N, the inclusion of weak interactions exhibited by the carbonyl oxygens of the arms, viz.,  $HgN_2O_2$ , leads to a geometry that best fits a distorted octahedron with two vacant sites. Even the recognition species of  $L_2$  with  $Ni^{2+}$  having the  $N_4O$  core can best be fitted to a distorted octahedron, but with one vacant site. The same receptor,  $L_2$  exhibits an  $N_4$  core with distorted tetrahedron for  $Zn^{2+}$ . However, when both  $Ni^{2+}$  and  $Zn^{2+}$  are present,  $Ni^{2+}$  goes predominantly to the nitrogen core (viz.,  $N_4$  and distorted tetrahedron) and  $Zn^{2+}$  goes predominantly to the oxygen core (viz.,  $O_5$  and distorted trigonal bipyramid). This seems to suggest that in hetero-bimetallo-proteins, selective preference of one metal ion over the other may play an important role in deciding which one should go to which position (binding core) in the protein. The vacant sites present in the metal binding core is a boon in these cases, since this indicates expandability of the coordination sphere, which in turn may favour occurrence of certain bioinorganic reactions.

Thus, the present study may provide some clues regarding the metal ion preferences in the metalloenzymes possessing several binding cores. The complexation of  $L_3$  by  $Cu^{2+}$  or  $Ag^+$ , exhibit distorted tetrahedral geometry with  $N_4$  core, indicating that it cannot selectively differentiate these two ions. The distorted tetrahedron can also be attributed to its easy of conversion to other geometries that may make it facile for catalytic reactions.

The  $Cu^{2+}$  complex of  $L_4$  exhibits distorted trigonal bipyramidal geometry wherein each arm of  $L_4$  acts as bidentate in filling a total of four coordinations, with the fifth coming from the acetonitrile, resulting in a  $NO_2S_2$  binding core. Even the species of recognition of  $L_5$  with  $Zn^{2+}$  having  $N_2O_2$  core provides a better fit to a trigonal bipyramidal with one trigonal center being vacant. The  $Cd^{2+}$  complex of the same receptor,  $L_5$  exhibits  $N_2O_4$  binding core to result in a capped octahedral geometry with one vacant site. While the  $Zn^{2+}$  binds at the Schiff base region, the  $Cd^{2+}$  binds primarily at the lower rim phenolic oxygen atoms. All these studies seem to suggest that selective preference of one metal ion over the other depends on the nature of the binding core as well the conformational mobility of the arms attached.

## References

- (a) Lucinat M & Ungaro R, *Calixarenes in Action*, (Imperial College Press, London) 2000; (b) Lumetta G J, Rogers R D, Gopalan A S, *Calixarenes for Separations*, (American Chemical Society, Washington DC) 2000; (c) Gutsche C D, *Aldrichim Acta*, 28 (1995) 3; (d) Gutsche C D, *Calixarenes Revisited* (Royal Society of Chemistry, Cambridge) 1998; (e) Ikeda A, Shinkai S, *Chem Rev*, 97 (1997) 1713; (f) McKerverey M A, Arnaud-Neu F, Schwing-Weill M J & Gokel G, *Comprehensive Supramolecular Chemistry*, vol 1, (Pergamon, Oxford) 1996, p. 537; (g) Pochini A, Ungaro R & Vögtle F, *Comprehensive Supramolecular Chemistry*, Vol 2, (Elsevier, Oxford) 1996, p. 103; (h) Böhmer V, *Angew Chem Int Ed Engl*, 34 (1995) 713.
- (a) Floriani C, *Chem Eur J*, 5 (1999) 19; (b) Floriani C & Floriani-Moro R, *Adv Organomet Chem*, 47 (2001) 167; (c) Wieser C, Dieleman C B & Matt D, *Coord Chem Rev*, 165 (1997) 93.
- (a) Gutsche C D, Levine J A, No K H & Bauer L, *Tetrahedron*, 39 (1983) 409; (b) Park K S, Jung S O, Lee S S & Kim J S, *Bull Korean Chem Soc*, 21 (1996) 909; (c) Kim J S & Quang D T, *Chem Rev*, 107 (2007) 3780; (d) Creaven B S, Donlon D F & McGinley J, *Coord Chem Rev*, 253 (2009) 893.
- Golebiowski J, Lamare V, Ruiz-Lo'pez M F, Asfari Z, Böhmer V, Harrowfield J M & Vicens J, *Calixarene 2001*, (Kluwer Academic, Dordrecht) 2001.
- (a) Dessingou J, Joseph R & Rao C P, *Tetrahedron Lett*, 46 (2005) 7967; (b) Acharya A, Ramanujam B, Chinta J P & Rao C P, *J Org Chem*, 76 (2011) 127; (c) Joseph R, Chinta J P & Rao C P, *J Org Chem*, 75 (2010) 3387; (d) Joseph R, Chinta J P & Rao C P, *Inorg Chim Acta*, 363 (2010) 2833; (e) Joseph R, Ramanujam B, Pal H & Rao C P, *Tetrahedron Lett*, 49 (2008) 6257; (f) Joseph R, Ramanujam B, Acharya A & Rao C P, *Tetrahedron Lett*, 50 (2009) 2735; (g) Joseph R, Ramanujam B, Acharya A & Rao C P, *J Org Chem*, 74 (2009) 8181; (h) Joseph R, Ramanujam B, Acharya A, Khutia A & Rao C P, *J Org Chem*, 73 (2008) 5745; (i) Joseph R & Rao C P, *Chem Rev*, 111 (2011), 4658.

- 6 (a) Gaussian 98, rev A.11.1, (Gaussian Inc, Pittsburgh, PA) 2001; (b) Gaussian 03, rev E. 01, (Gaussian Inc, Wallingford, CT) 2004.
- 7 Zhurko G A & Zhurko D A, *Chemcraft*, <http://www.chemcraftprog.com>, 2006.
- 8 GaussView 3.0 (Gaussian Inc, Pittsburgh, PA) 2003.
- 9 (a) Anders E, Koch R & Freunsch P, *J Comp Chem*, 14 (1993) 1301; (b) Dewar M J S & Holder A J, *Organometallics*, 9 (1990) 508; (c) Dewar M J S & Jie C, *J Mol Struct (Theochem)*, 187 (1989) 1; (d) Dewar M J S, Jie C & Zebisc E G, *Organometallics*, 7 (1988) 513; (e) Dewar M J S, McKee M L & Rzepa H S, *J Am Chem Soc*, 100 (1978) 3607; (f) Dewar M J S & Merz K M, *Organometallics*, 7 (1988) 522; (g) Dewar M J S & Reynolds C H, *J Comp Chem*, 2 (1986) 140; (h) Dewar M J S & Thiel W, *J Am Chem Soc*, 99 (1977) 4499; (i) Dewar M J S & Yuan Y C, *Inorg Chem*, 29 (1990) 3881; (j) Dewar M J S, Zebisch E G & Healy E F, *J Am Chem Soc*, 107 (1985) 3902.
- 10 (a) Stewart J J P, *J Comp Chem*, 10 (1989) 209; (b) Stewart J J P, *J Comp Chem*, 10 (1989) 221.
- 11 (a) McWeeny R & Dierksen G, *J Chem Phys*, 49 (1968) 4852; (b) Pople J A & Nesbet R K, *J Chem Phys*, 22 (1954) 571; (c) Roothan C C J, *Rev Mod Phys*, 23 (1951) 69.
- 12 (a) Collins J B, Schleyer P v R, Binkley J S & Pople J A, *J Chem Phys*, 64 (1976) 5142; (b) Hehre W J, Stewart R F & Pople J A, *J Chem Phys*, 51 (1969) 2657.
- 13 (a) Binkley J S, Pople J A & Hehre W J, *J Am Chem Soc*, 102 (1980) 939; (b) Dobbs K D & Hehre W J, *J Comp Chem*, 7 (1986) 359; (c) Dobbs K D & Hehre W J, *J Comp Chem*, 8 (1987) 880; (d) Dobbs K D & Hehre W J, *J Comp Chem*, 8 (1987) 861; (e) Gordon M S, Binkley J S, Pople J A, Pietro W J & Hehre W J, *J Am Chem Soc*, 104 (1982) 2797; (f) Pietro W J, Francl M M, Hehre W J, Defrees D J, Pople J A & Binkley J S, *J Am Chem Soc*, 104 (1982) 5039.
- 14 (a) Binning Jr R C & Curtiss L A, *J Comp Chem*, 11 (1990) 1206; (b) Blaudeau J P, McGrath M P, Curtiss L A & Radom L, *J Chem Phys*, 107 (1997) 5016; (c) Ditchfield R, Hehre W J & Pople J A, *J Chem Phys*, 54 (1971) 724; (d) Gordon M S, *Chem Phys Lett*, 76 (1980) 163; (e) Hariharan P C & Pople J A, *Theor Chim Acta*, 28 (1973) 213; (f) Hariharan P C & Pople J A, *Mol Phys*, 27 (1974) 209; (g) Hehre W J, Ditchfield R & Pople J A, *J Chem Phys*, 56 (1972) 2257; (h) Rassolov V A, Pople J A, Ratner M A & Windus T L, *J Chem Phys*, 109 (1998) 1223; (i) Rassolov V A, Ratner M A, Pople J A, Redfern P C & Curtiss L A, *J Comp Chem*, 22 (2001) 976.
- 15 (a) Dunning Jr T H & Hay P J, *Modern Theoretical Chemistry*, Vol. 3, edited by H F Schaefer III, (Plenum, New York) 1976, p. 1; (b) Fuentealba P, Preuss H, Stoll H & Szentpaly L V, *Chem Phys Lett*, 89 (1989) 418; (c) Fuentealba P, Stoll H, Szentpaly L V, Schwerdtfeger P & Preuss H, *J Phys B*, 16 (1983) 1323; (d) Fuentealba P, Szentpaly L V, Preuss H & Stoll H, *J Phys B*, 18 (1985) 1287; (e) Szentpaly L V, Fuentealba P, Preuss H & Stoll H, *Chem Phys Lett*, 93 (1982) 555; (f) Stoll H, Fuentealba P, Schwerdtfeger P, Flad J, Szentpaly L V, Preuss H, *J Chem Phys*, 81 (1984) 2732; (g) Wedig U, Dolg M, Stoll H & Preuss H, in *Quantum Chemistry: The Challenge of Transition Metals and Coordination Chemistry*, edited by A Veillard (D Reidel, Dordrecht) 1986, p. 79; (h) Dolg M, Fulde P, Kuechle W, Neumann C S & Stoll H, *J Chem Phys*, 94 (1991) 3011; (i) Dolg M, Stoll H, Flad H J & Preuss H, *J Chem Phys*, 97 (1992) 1162; (j) Dolg M, Stoll H & Preuss H, *J Chem Phys*, 90 (1989) 1730; (k) Dolg M, Stoll H & Preuss H, *Theor Chim Acta*, 85 (1993) 441; (l) Dolg M, Stoll H, Preuss H & Pitzer R M, *J Phys Chem*, 97 (1993) 5852; (m) Dolg M, Stoll H, Savin A & Preuss H, *Theor Chim Acta*, 75 (1989) 173; (n) Dolg M, Wedig U, Stoll H & Preuss H, *J Chem Phys*, 86 (1987) 866; (o) Igelmann G, Stoll H & Preuss H, *Mol Phys*, 65 (1988) 1321; (p) Schwerdtfeger P, Dolg M, Schwarz W H E, Bowmaker G A & Boyd P D W, *J Chem Phys*, 91 (1989) 1762; (q) Andrae D, Haeussermann U, Dolg M, Stoll H & Preuss H, *Theor Chim Acta*, 77 (1990) 123; (r) Kaupp M, Schleyer P V R, Stoll H & Preuss H, *J Chem Phys*, 94 (1991) 1360; (s) Kuechle W, Dolg M, Stoll H & Preuss H, *Mol Phys*, 74 (1991) 1245; (t) Kuechle W, Dolg M, Stoll H & Preuss H, *J Chem Phys*, 100 (1994) 7535; (u) Bergner A, Dolg M, Kuechle W, Stoll H & Preuss H, *Mol Phys*, 80 (1993) 1431; (v) Haeussermann U, Dolg M, Stoll H & Preuss H, *Mol Phys*, 78 (1993) 1211; (w) Nicklass A, Dolg M, Stoll H & Preuss H, *J Chem Phys*, 102 (1995) 8942; (x) Leininger T, Nicklass A, Stoll H, Dolg M & Schwerdtfeger P, *J Chem Phys*, 105 (1996) 1052; (y) Cao X Y & Dolg M, *J Chem Phys*, 115 (2001) 7348; (z) Cao X Y & Dolg M, *J Mol Struct (Theochem)*, 581 (2002) 139.
- 16 (a) Hay P J & Wadt W R, *J Chem Phys*, 82 (1985) 270; (b) Hay P J & Wadt W R, *J Chem Phys*, 82 (1985) 299; (c) Wadt W R & Hay P J, *J Chem Phys*, 82 (1985) 284.
- 17 Grabowski S J, *Annu Rep Prog Chem, Sect C*, 102 (2006) 131.
- 18 (a) Cundari T R & Stevens W J, *J Chem Phys*, 98 (1993) 5555; (b) Stevens W, Basch H & Krauss J, *J Chem Phys*, 81 (1984) 6026; (c) Stevens W J, Krauss M, Basch H & Jasien P G, *Can J Chem*, 70 (1992) 612.
- 19 Jian F F, Zhao P S & Ma H B, *Struct Chem*, 16 (2005) 469.
- 20 (a) Danil de Namor A F, Aguilar-Cornejo A, Sonalhi R, Shehab M, Nolan K B, Ouazzani N & Mandi L, *J Phys Chem B*, 109 (2005) 14735; (b) García-Raso Á, Fiol J J, Rigo S, López-López A, Molins E, Espinosa E, Borrás E, Alzuet G, Borrás J & Castiñeiras A, *Polyhedron*, 19 (2000) 991; (c) Golzar Hossain G M, Amoroso A J, Banu A & Malik K M A, *Polyhedron*, 26 (2007) 967; (d) Marques L, de L, Lang E S, Fenner H & Castellano E E, *Z Anorg Allg Chem*, 631 (2005) 745; (e) Meyer G & Nockemann P, *Z Anorg Allg Chem*, 629 (2003) 1447.
- 21 (a) Biswas S, Mostafa G, Steele I M, Sarkar S & Dey K, *Polyhedron*, 28 (2009) 1010; (b) Deacon G B, Forsyth C M, Junk P C, Ness T J, Izgorodina E, Baldamus J, Meyer G, Pantenburg I, Hitzbleck J & Ruhlandt-Senge K, *Eur J Inorg Chem*, (2008) 4770; (c) Mendizabal F, Burgos D & Oleazar C, *Chem Phys Lett*, 463 (2008) 272; (d) Rofouei M K, Beiza A & Gharamaleki J A, *Acta Cryst E*, 65 (2009) m1259.
- 22 (a) Amiri A, Amirnasr M, Meghdadi S, Mereiter K, Ghodsi V & Gholami A, *Inorg Chim Acta*, 362 (2009) 3934; (b) Efthymiou C G, Papatriantafyllopoulou C, Alexopoulou N I, Raptopoulou C P, Boča R, Mrozinski J, Bakalbassis E G & Perlepes S P, *Polyhedron*, 28 (2009) 3373; (c) Papatriantafyllopoulou C, Estrader M, Efthymiou C G, Dermizaki D, Gkotsis K, Terzis A, Diaz C & Perlepes S P, *Polyhedron*, 28 (2009) 1652.
- 23 (a) Das A K, Gowda N S, Botoshansky M, Sridhar M A, Kaftory M & Sashidhara Prasad J, *J Mol Struct*, 938 (2009) 259; (b) Qiao C, Li J, Xu Y, Guo S, Qi X & Fan Y, *J Coord Chem*, 62 (2009) 3268; (c) Shahid M, Rüffer T, Lang H, Awan S A & Ahmad S, *J Coord Chem*, 62 (2009) 440.

- 24 Inoue T, Sugawara H, Hamanaka S, Tsukui H, Suzuki E, Kohzuma T & Kai Y, *Biochemistry*, 38 (1999) 6063.
- 25 Schmittel M, He B, Fan J, Bats J W, Engeser M, Schlosser M & Deiseroth H -J, *Inorg Chem*, 48 (2009) 8192.
- 26 Abu-Youssef M A M, Dey R, Gohar Y, Massoud A A, Öhrström L & Langer V, *Inorg Chem*, 46 (2007) 5893.
- 27 Birker P J M W L, Helder J, Henkel G, Krebs B & Reedijk J, *Inorg Chem*, 21 (1982) 357.
- 28 (a) Arslan F, *Dyes Pigments*, 75 (2007) 521; (b) Chand B G, Ray U S, Cheng J, Lu T -H & Sinha C, *Polyhedron*, 22 (2003) 1213; (c) Wang Y, Zhang X, Zhang Q & Yang Z, *Biometals*, 2 (2010) 265.
- 29 (a) Xia S Q, Hu S M, Zhang J J, Wu X T, Dai J C, Fu Z Y & Du W X, *Inorg Chem Commun*, 7 (2004) 271; (b) Xu X Y, Chen J L, Luo Q H, Shen M C, Huang X Y & Wu Q J, *Polyhedron*, 16 (1997) 223.